Stabilization mechanisms of an ammonia/methane non-premixed jet flame up to liftoff.

Sophie Colson, Manuel Kuhni, Akihiro Hayakawa, Hideaki Kobayashi, Cédric Galizzi, Dany Escudie

Stabilization mechanisms of an ammonia/methane non-premixed jet flame up to liftoff.

Sophie Colson[1,2,*], Manuel Kuhni[1], Akihiro Hayakawa[2], Hideaki Kobayashi[2], Cédric Galizzi[1], Dany Escudié[1]

[1] Univ Lyon, INSA-Lyon, CNRS, CETHIL UMR5008, 69621 Villeurbanne, France

[2] Institute of Fluid Science, Tohoku University, 2-1-1 Katahira, Aoba-ku, Sendai 980-8577, Japan

Abstract: Ammonia is a promising alternative fuel for CO_2 emission mitigation. The use of ammonia blends allows for more flexibility compared to pure ammonia fuel and is often considered for immediate CO_2 emission reduction in existing facilities running on natural gas. However, fundamental studies on these fuel mixtures remain scarce. This study thus focuses on ammonia/methane blend fuels. The effect of ammonia on methane jet flame stabilization is investigated using a non-premixed jet flame configuration to observe the flame stabilization mechanisms, the flame-burner interactions and how ammonia addition affects the attached flame stabilization up to liftoff. The flame tip position was observed using CH* chemiluminescence. Heat transfer to the burner was monitored by temperature measurement at

* corresponding author: colson.sophie@tohoku.ac.jp

the burner lip and inside the burner to observe the impact of ammonia addition on thermal interactions. The main stabilization regimes described for the methane non-premixed jet flame are still observed in the case of ammonia addition. However, the transition between those regimes appeared to be shifted toward larger velocities relative to the methane case due to ammonia addition. Those changes could be related to the change in the mixture combustion properties which affects both flame position, heat transfer to the burner and in turn the transition between the identified stabilization regimes. The dynamic leading to liftoff was further analyzed to highlight how ammonia addition perturbated the stabilization balance up to liftoff.

Keywords: non-premixed jet flame; stabilization; ammonia/methane; flame-burner thermal interaction, liftoff process

Nomenclature

r	radial direction (r = 0 at the burner center axis) [mm]
z	axial direction (z = 0 at the burner lip surface) [mm]
(R_a, H_a)	Flame base attachment position (radius, height) [mm]
(R_E, H_E)	Flame base extremum position (radius, height) [mm]
($R_{L\text{-}T}$, $H_{L\text{-}T}$)	Flame base position at laminar to turbulent transition (radius, height) [mm]
(R_{LO}, H_{LO})	Flame base position just before liftoff (radius, height) [mm]
d_a	Distance flame-burner lip [mm]
L	Length of the fuel injection pipe [mm]
D_i	Inner diameter of the fuel injection pipe [mm]
e	Burner lip thickness [mm]
U_J	Jet velocity [m·s^{-1}]
U_{co}	Coflow velocity [m·s^{-1}]
U_{LO}	Jet velocity at liftoff [m·s^{-1}]
E	Ammonia mixing ratio
X_i	Mole fraction of specie i in fuel mixture
LHV_i	Lower heating value of specie i [kJ·mol^{-1}]

Φ	Conduction heat flux in the burner lip, assuming unidirectional conduction [kW·m^{-2}]
λ	Thermal conductivity of the burner, for temperature corresponding to the mean temperature between T_{lip} and T_{6mm} [W·m^{-1}·K^{-1}]
T_{lip}	Burner lip temperature, at the lip surface (z = 0 mm) [K]
T_{6mm}	Burner temperature at 6 mm under the lip surface (z = - 6 mm) [K]
S_{L0}	Unstretched laminar burning velocity at T = 298 K, 1 atm and ϕ = 1.0 [m·s^{-1}]
T_{ad}	Adiabatic flame temperature [K]
Le_F	Fuel Lewis number
Le_{eff}	Effective Lewis number as defined in [1] for diffusion flames
Z_{st}	Stochiometric mixing fraction
MR	Momentum Ratio
Re_J	Jet Reynolds number
Re_{lip}	Local Reynolds number in the wake of the burner lip

1. Introduction

Ammonia has attracted recent attention for its use as a carbon-free energy carrier [2,3]. Indeed, ammonia presents interesting features that make it both cost-effective and fastly and broadly deployable for the energy industry [4,5]. Though its production is for now mainly carbon-based, green-ammonia production is possible using water and nitrogen, employing water electrolysis and Haber-Bosh process as a way to store energy from renewable resources. This green ammonia can be later used as a fuel in various combustion situations ranging from SI engines to gas turbine applications [6–8]. However, some major challenges remain including the NOx emission and flame stabilization issues. Regarding the stabilization issue, the use of fuel blends can be considered, such as ammonia/hydrogen mixtures or ammonia/hydrocarbons mixtures, with a greater reactivity than the pure ammonia, therefore easing stabilization. Among those blends, ammonia/hydrocarbons mixing are essential for short-term CO_2 emission mitigation strategy through the addition of ammonia in existing facilities currently running on hydrocarbons. The combustion properties of those blends had thus recently attracted attention [9–12]. However, studies on those blend fuel flame stabilization mechanisms remain scarce. Among them, Hayakawa et al. [13] studied the flame stabilization domain in a swirl burner for premixed ammonia flame. A more fundamental approach was taken by Rohdes et al. [14] observing a premixed ammonia turbulent flame stabilized on a flame holder, doped with O_2.

This work focuses on the stabilization mechanisms and the flame-burner interactions of an ammonia/methane flame using a non-premixed jet flame configuration in air coflow. A local approach is considered in the present work, focusing on the stabilization mechanisms up to liftoff, and completing the global approach and the characterization of the jet stabilization domain performed in a previous study [15].

The non-premixed jet flame configuration has been used in many fundamental studies on flame stabilization as reviewed by Lyons or Lawn [16,17]. This academic configuration is relatively simple and allows to look at the detail of the mechanisms of flame stabilization, from a global approach [18,19] to a more local approach close to flame tip [20–24]. In the present configuration, and as developed in our previous work [15] we describe the evolution of the stabilization domain of a methane flame with ammonia addition. In the following, we will refer to “liftoff” as the transition between attached and lifted flames, “blowout” as the transition from lifted flames to extinction, “re-attachment” as the transition from lifted flames to attached flames and finally “blowoff” as direct extinction from attached flames. In our previous work [15], ammonia addition led to a particularly large decrease of the liftoff limit, with direct blowoff observed close to 50% of ammonia in terms of mole fraction in the fuel mixture. Chemical effects are expected to be dominant, as observed from the particularly large decrease in the laminar burning velocity when ammonia is added to the fuel mixture. Nonetheless, the

predominance of the chemical aspects on flame stabilization may depend on the ammonia content in the mixture, relatively to other parameters such as thermal or diffusive ones. The study of global parameters alone could not explain satisfactorily the large decrease observed, and a more local and dynamic approach, focusing on the flame tip (leading edge), is thus considered in the present work to observe the evolution with ammonia addition of the aero-thermo-chemical coupling at the burner lip up to liftoff.

The objective of the present work is to clarify how flame stabilization is impacted by the addition of ammonia in the fuel mixture by looking at the evolution of the flame local stabilization dynamics and its interaction with the burner when adding ammonia, completing our previous global approach [15].

2. Experimental setup

2.1.Setup Overview

The flame stabilization was studied using a non-premixed jet flame configuration as represented in Fig. 1. The setup is constituted of a pipe for fuel injection of inner diameter, D_i, 6 mm, and lip thickness, e, of 2 mm. Pipe length, L, is 950 mm, ensuring a ratio $L/D_i > 150$. This pipe exits in a closed squared chamber of 250 x 250 mm^2. The oxidizer, air in this study, is going through perforated plates and a convergent to insure a well-relaminarized profile at the burner outlet. Velocity profiles at the burner outlet were observed using laser doppler anemometry

measurements in previous work [22] and the mean jet velocity, U_J, obtained from the mass flow rate was shown to be in satisfactory agreement with those measurements (within 6 % error). In the present work the coflow velocity, U_{co}, was set to 0.2 m·s^{-1}, corresponding to the largest stabilization domain up to blowoff in the range of U_{co} = 0 – 0.3 m·s^{-1} accessible [15].

Methane and ammonia are mixed before injection in the setup. The ratio of ammonia to methane in the fuel mixture is defined in Eq. (1) using the ammonia mixing ratio, E, as in previous work [9,10],

$$E = \frac{X_{NH_3} \cdot LHV_{NH_3}}{X_{NH_3} \cdot LHV_{NH_3} + X_{CH_4} \cdot LHV_{CH_4}} \quad (1)$$

where X_i is the mole fraction of fuel i in the fuel mixture and LHV_i is the lower heating value of i, with LHV_{CH4} = 802.3 kJ·mol^{-1} and LHV_{NH3} = 316.8 kJ·mol^{-1}.

The flow rate of each gas is controlled and monitored by thermal mass flow controllers (SLA5850 series, Brooks Instrument Co., Hatfield, PA, USA) with a precision of 0.7 % of the mass flow rate, more 0.2 % of the full range, leading by propagation to a maximal uncertainty of 2 % on the velocities and 3 % on the ammonia mixing ratio, E.

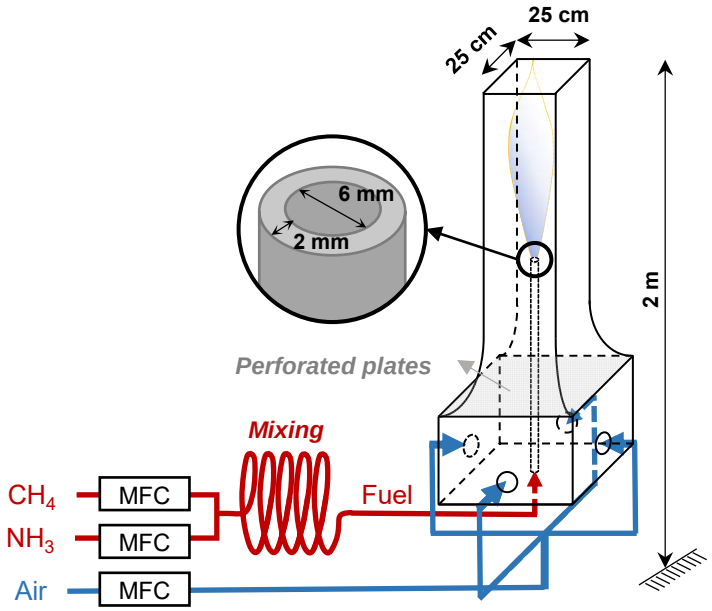

Figure 1. Experimental setup overview.

In this study, the dynamics of the attached flame up to liftoff was observed for E varying between 0 and 0.3, near the direct blowoff case as developed in previous work [15]. The range of jet velocity, U_J, explored thus cover values from 0.05 m·s^{-1} to 16 m·s^{-1}.

2.2. Observations at the burner lip.

To analyze the local dynamics of the attached flame and how the aero-thermo-chemical balance is broken at liftoff, several local measurements were performed at the burner lip. The attached flame position was observed using CH* chemiluminescence imaging. CH* is known to be a good marker of the largest heat release rate region within the flame front and has been used in several works on methane/hydrocarbons flame [25]. Besides, from 1D simulations on

ammonia/methane non-premixed flames, shown in the supplementary material section of this work, it can be seen that CH radicals remain a good marker for the heat release zone for ammonia/methane mixtures. The spatial variation between the CH distribution peak and the heat release rate peak being smaller than the spatial resolution achievable in the present work, CH* was selected as a marker of the HRR region. Other markers, such as NH*, presented lower intensity in the range of ammonia mixing ratio, E, investigated and were thus not considered in the present study.

The CH* chemiluminescence was collected using an intensified camera (Teledyne Princeton Instruments PI-MAX 2) with an exposure time of 7 ms and a gain of 120. Series of 300 images were collected for each condition.

When introducing ammonia in the flame, the CH* chemiluminescence intensity is expected to decrease due to the smaller amount of CH* in the reaction region. Thus, the intensity was normalized by its maximum value on each image before post-processing. The 2D image of the front was retrieved from the 3D CH* chemiluminescence using Abel deconvolution [26]. Similar filtering was applied to all images. Detection of the flame attachment position was then performed by detection of a threshold of 45 % for the attachment height, H_a. Then at height H_a, the attachment radius, R_a, was detected with a threshold of and 40 %. These threshold values were selected to ensure proper detection of the attachment position for all the ammonia mixing

ratio, E, and jet velocity, U_J, conditions investigated, including the cases of lower signal to noise ratio due to lower CH* emissions. An example of a raw image and a post-processed image is represented in Fig 2. R_a and H_a were determined for each image of the set of 300 images, and the value reported in the following corresponds to the maximum of the statistical distribution observed. The distribution span is represented by the mean of error bar in the following, including both flame position fluctuations due to physical flame instability and uncertainty due to the measurement (particularly a smaller signal to noise ratio might contribute to a larger distribution span). Further details on the post-processing can be found in the supplementary material section.

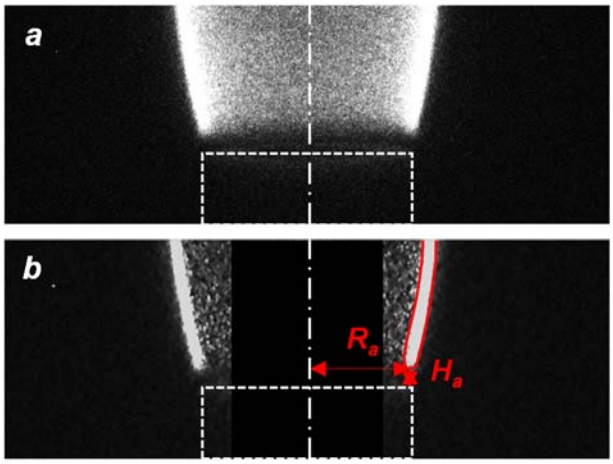

Figure 2. Chemiluminescence imaging and post-processing: (a) raw image; (b) post-processed image.

In addition to the attached flame position dynamics, the thermal interactions with the burner

were monitored by the mean of two K-thermocouples (Chromel - Alumel, 75 µm diameter in a sleeve of 0.5 mm) inside the burner lip as represented in Fig. 3. Those thermocouples enable to monitor the temperature at the lip surface, T_{lip}, and the one 6 mm under the lip surface, T_{6mm}, and the calculation of the conductive heat flux in the burner, Φ. Assuming unidirectional conduction, this heat flux, Φ, is obtained using the following Eq. (2)

$$\Phi = \lambda \cdot \frac{T_{lip} - T_{6mm}}{\Delta z} \qquad (2)$$

Where λ is the conductivity of the burner lip (Al_2O_3) at $(T_{lip} + T_{6mm})/2$ and Δz = 6 mm is the distance between the hot junctions of the two thermocouples.

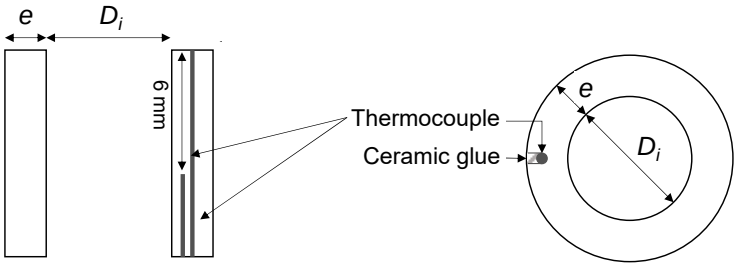

Figure 3. Burner lip and thermocouple positions.

Finally, a temperature mapping of the flame was performed using an R-type thermocouple (Pt-Pt/Rh13%, 50 µm diameter). This temperature mapping was performed in the direct vicinity of the burner lip at a height, z, between 2 mm and 8 mm above the burner lip, and a radius, r, between 0 and 15 mm. This mapping was used to observe the flame temperature variations and temperature distribution near the burner and how they varied with ammonia addition and jet

velocity change. Radiative heat losses and heat losses by conduction to the thermocouple were not considered in the present work as only relative evolution was considered for qualitative analysis and not for absolute measurement. Details on the thermocouple and its interactions with the flame are available in the supplementary material section. The direct, uncorrected, temperature measurement gave maximum temperature for the velocity range investigated between 1850 K and 1950 K for $E = 0$, and 1840 K and 1870 K for $E = 0.3$, and are in agreement with previous work [27, 28]

3. Results and discussion

3.1. Flame local stabilization dynamics

Local study of the flame stabilization in the present configuration was done in previous work [28] in the case of a methane flame with a focus on thermal aspects, with preheating of the oxidizer, from low jet velocity in the laminar regime and up to liftoff. This previous work describes the evolution of the flame tip position, burner temperature and heat flux up to liftoff, and defined 3 main regimes of stabilization as briefly recalled in the following and summarized in Fig. 4:

- *Regime I:* the flame moves toward the oxidizer and downward as the jet velocity is increased up to an extremum position (R_E, H_E). This first regime corresponds to the gradual expansion of the jet as U_J is increased up to a momentum ratio, *MR*, in the range 3-7,

corresponding to the extremum position.

- *Regime II:* From the extremum position (R_E, H_E), if U_J is further increased, the flame will move back toward the fuel jet, as an increased jet velocity drags air in the wake of the burner lip, changing the local fuel and oxidizer concentration, and moving the stoichiometric line $Z = Z_{st}$ closer to the jet centreline. In this regime, the temperature at the burner lip keeps decreasing due to enhanced heat transfer.
- *Regime III:* The last regime observed before liftoff corresponds to laminar to turbulent transition in the pipe, $Re_J = U_J \cdot D_i / \nu$, with ν the kinematic viscosity of the fuel mixture. From that transition point ($R_{L\text{-}T}$, $H_{L\text{-}T}$), the flame tip keeps moving toward the centreline as more air is dragged in the wake of the burner lip, but flame attachment height slightly decreases. The temperature at the burner lip further drops as convection is emphasized.

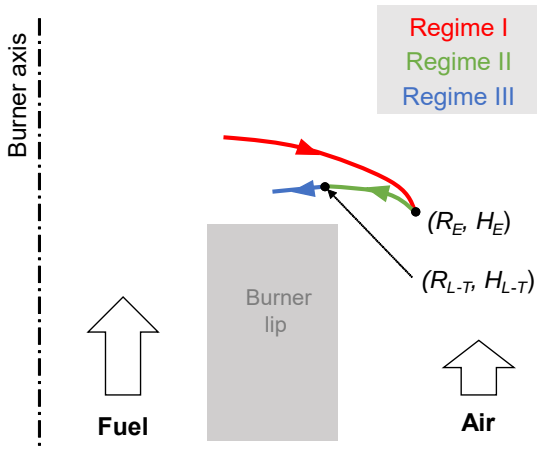

Figure 4. Sketch representing the attached flame stabilization regimes as introduced by Lamige et al. [28].

The regime I can be further subdivided into two regimes Ia and Ib, corresponding to a change in the thermal interaction with the burner lip. In region Ia, the flow is assumed to be purely viscous in the wake of the burner lip and heat transfer dominated by conduction. As the jet velocity, U_J, is increased, heat transfer by convection becomes more important, corresponding to regime Ib. This change is observable in the evolution of the temperature at the burner lip, T_{lip}, and the conductive heat flux in the burner lip, Φ [28]. When U_J is increased, T_{lip} increases and reaches a maximum before decreasing. This maximum corresponds to the transition from Ia to Ib. The conductive heat flux Φ in the burner calculated from the thermocouples measurements confirms this analysis with an increase in Φ in regime Ia, stabilizing in region Ib before decreasing in regime II, for which air recirculation appears, and further decreasing when entering regime III, as the jet becomes turbulent. A local Reynolds number, $Re_{lip} = U_J \cdot e / \nu_{lip}$, was thus introduced, characterizing the transition Ia to Ib, with U_J, the jet velocity, e, the burner lip thickness and ν_{lip} the local viscosity calculated for a stoichiometric mixture at T_{lip}. In the case of methane, the transition from Ia to Ib was shown to be close to 10 [28].

The introduction of ammonia in the jet leads to several changes in terms of thermal properties, diffusive properties and fundamental combustion characteristics as introduced in Table 1, where ammonia mixing ratio, E, and ammonia mole fraction in fuel mixture, X_{NH3}, are first recalled. It

could be observed in previous work that, though the flame is considered as mostly diffusive, partial premixing is assumed to occur in the dark region close to the burner, enabling the leading edge of the flame to develop in the vicinity of the burner, with higher heat release rates and supporting the diffusion trail [21,23,24]. As a first approach, the laminar burning velocity of a stoichiometric ammonia/methane/air premixed flame, S_{L0}, is reported in Table 1. As ammonia is added S_{L0} decreases, reflecting the lower reactivity of the mixture observed for larger ammonia content. This decrease is expected to play an important role in flame destabilization [24] and the diminution of the liftoff velocity, U_{LO}, as developed in previous work [15]. Other parameters are also expected to affect the local flame stabilization. The flame adiabatic temperature decreases by close to 70 K when ammonia is introduced up to $E = 0.3$, while the maximum heat released by the flame is divided by 3. This might drive changes in the thermal interaction with the burner, affecting in turn flame stabilization. The thermo/diffusive balance is also introduced in Table 1 with the effective Lewis number, $Le_{eff} = (Le_F + A_f \cdot Le_{O2}) / (1+A_f)$, calculated as in [1], taking into account both the effective Lewis number of the fuel, Le_F, and oxidizer, Le_{O2}, and the parameter $A_f = aY_F/Y_O$ with a the stoichiometric oxidizer-to-fuel mass ratio, and Y_F and Y_O the fuel and oxidizer mass fractions. The variation of Le_{eff} in the range of mixture investigated remains moderated and close to unity. Finally, the change in the fuel also leads to a change in the stoichiometric mixing fraction, Z_{st}, which is expected to influence the flame position and the

local stabilization balance.

Table 1. Some fundamental combustion parameters for methane/ammonia mixtures.

E **Ammonia mixing ratio**	**0**	**0.1**	**0.2**	**0.3**
X_{NH3} Ammonia fuel mixing mole fraction	0	0.22	0.39	0.52
S_{L0} [m.s^{-1}] Laminar burning velocity at stoichiometric condition from experiment [11]	0.35	0.27	0.22	0.19
T_{ad} [K] Adiabatic temperature Stoichiometric, calculation from PREMIX code [9,29]	2229	2194	2174	2157
HRR_{max} [J.m^{-3}.s^{-1}] Maximum heat release rate Stoichiometric, calculation from PREMIX code [9,29]	4.31E9	2.71E9	1.94E9	1.43E9
Le_{eff} Effective Lewis number for diffusion flame From [1]	1.113	1.107	1.101	1.096
Z_{st} Stoechiometric mixture fraction	0.0552	0.0642	0.0731	0.082

To investigate how those changes will affect the flame-burner interaction, the evolution of the local stabilization dynamic of the flame (flame position, burner temperature and heat transfer to the burner) was observed with progressive addition of ammonia, taking the regimes detailed earlier for pure methane flame as a reference.

3.2. Effect of ammonia addition on flame position

The effect of ammonia addition on flame stabilization is first observed looking at the attached flame position evolution with ammonia addition. The attachment radius, R_a, and the attachment height, H_a, are represented in Fig. 5 for ammonia methane mixing ratio from $E = 0$ to $E = 0.3$ as a function of MR, the momentum ratio of fuel and air defined as criteria for the transition from the regime I to regime II as previously developed in the case of a methane flame.

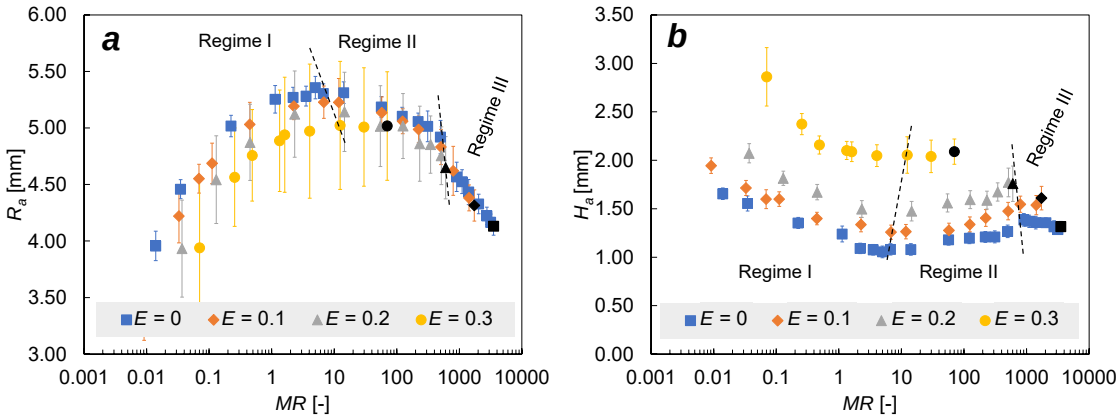

Figure. 5. Evolution of flame tip height and radius with gradual ammonia addition: (a) Attachment radius, R_a; (b) Attachment height, H_a. The position just before liftoff is highlighted by black symbol.

From Figure 5, it can be observed that the global evolution of the attached flame as described in the introduction of this work is still valid for this type of mixture, with the simultaneous observation of maximum of R_a and minimum of H_a corresponding to the transition from I to II and the position (R_E, H_E). For low ammonia content ($E < 0.2$), the transition II to III is still

observed with a change in the variation of H_a and a larger decreasing slope for R_a is observed for jet velocity such as $Re_J > 2300$. For larger ammonia content though, the liftoff occurred before the jet laminar to turbulence transition occurred at $Re_J = 2300$.

In addition, the introduction of ammonia lead to a decrease in R_a, and an increase in H_a for all the jet velocity condition U_J explored (respectively MR, Re_J).

Looking further in the evolution of R_a and H_a, it is worth noticing in Fig. 5 that, though the 3 regimes are still observed, the transition between regime I and II, corresponding to the flame extremum position (R_E, H_E), appears for a gradually higher MR_E as ammonia is introduced, from $MR_E = 5$ ($U_{JE} = 0.61$ m/s) for $E = 0$ to $MR_E = 20$ ($U_{JE} = 1.2$ m/s) for $E = 0.3$. The evolution of the flame position and the transitions between the identified stabilization regime with MR (as well as U_J or R_{eJ}) is varying with E.

To understand this increase in MR_E, it is necessary to go back to the physical change corresponding to this transition. The transition from regime I to II corresponds to the motion of the stoichiometric line toward the jet due to the air dragged in the wake of the lip by larger jet velocity. This transition has been associated with a momentum ratio of 3 - 7 in a previous study on methane flame [28]. Nonetheless, this parameter remains global and does not take into account the eventual local variations of the stoichiometric mixture line due to air drag. One explanation for the increase of MR_E when ammonia is introduced is to relate to the higher flame

position, as represented in the sketch in Fig 6. The impact of the air dragged on the Z contour is expected to gradually become more important as the velocity is increased, with at first small impact relatively close to the burner, and then gradually more pronounced, with streamlines gradually going further toward the jet axis. The difference in MR_E observed for the point of transition might be attributed to the fact that for greater ammonia content, larger jet velocity is necessary to drag sufficient air to change the stoichiometric line Z_{st} up to the position at which is stabilized the flame.

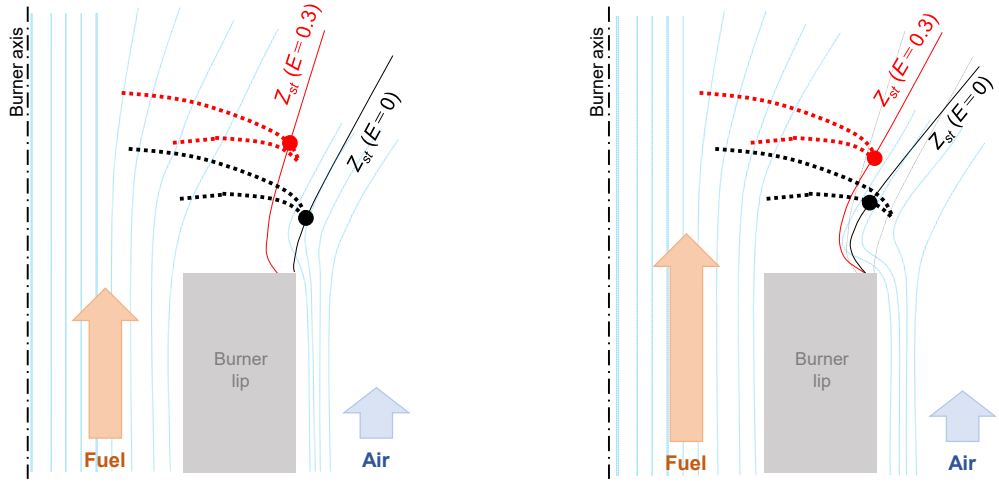

(a) $MR = MR_E\,(E = 0) < MR_E\,(E = 0.3)$ **(b)** $MR = MR_E\,(E = 0.3) > MR_E\,(E = 0)$

Figure. 6. Schematics explaining the evolution of the I to II transition (extremum position): (a) transition for $E = 0$; (b) Transition for $E = 0.3$.

Taking this extremum position as a reference, as represented in Fig. 7, it can be seen that the flame positions for different mixtures are overlapping, except for some particularly low-velocity

conditions. The complete evolution of the flame position for increasing U_J can then be described referring to the methane flame case, and the evolution on R_a and H_a with ammonia addition limited to the observation of the evolution of the extremum (R_E, H_E).

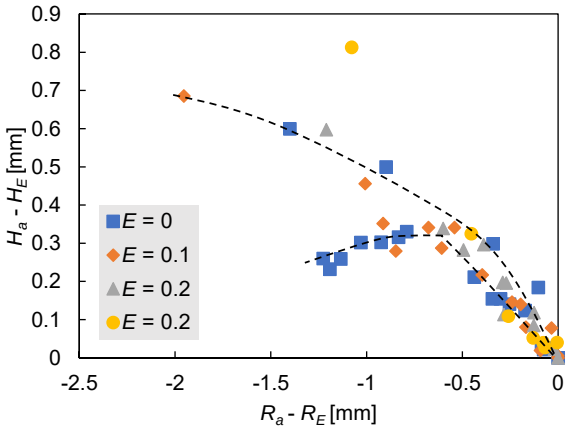

Figure 7. Flame position for various U_J relative to the extremum position (R_E, H_E) for E = 0, 0.1, 0.2 and 0.3.

The decrease of R_E can be attributed to the change in the Z_{st} with ammonia addition. Indeed, when ammonia is added Z_{st} is increased as recalled in Table 1. Thus, for a similar jet/coflow momentum ratio MR, the location of the mixture contour, $Z = Z_{st}$, called in the following stoichiometric line, is moving toward the jet. For the same MR value, an ammonia/methane flame is thus closer to the jet centerline and R_E is reduced as ammonia is added. A strong correlation between R_E and Z_{st} is thus observed in the present data as shown in Fig. 8, relating the radius of the flame normalized by the burner lip thickness, $[R_E - (D_i/2)]/e$, with the

stoichiometric mixing fraction Z_{st}. Extrapolation of this relation for other jet configurations is however subject to caution, as the geometry of the burner outlet, particularly the lip, might greatly affect the local velocity flow field and the distribution of the *Z*-contours. Generalization of such relation would require the actual measurement of mixing fraction *Z* in the wake of the burner lip and its direct surrounding, to derive a more accurate relationship. Such type of measurement is however extremely complex in practice, considering the fuel involved and the burner dimension.

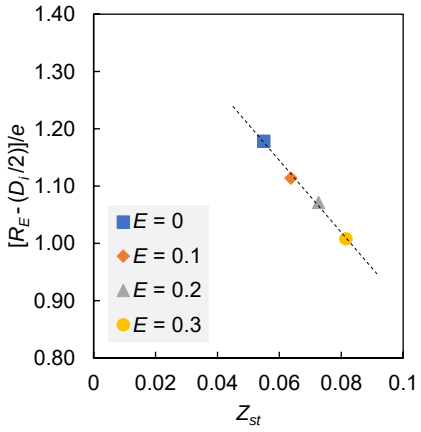

Figure 8. Correlation flame radius – stoichiometric mixture fraction Z_{st} for various E.

Several interpretations of the evolution of H_E with ammonia addition can be done. Following the leading-edge theory and considering partial premixing at the flame tip, the reduction of the local flame speed, due to the lower reactivity of ammonia as observed from its lower laminar burning velocity in Table 1, is expected to be one of the reasons of the higher attachment

position. For a constant *MR*, the flame is thus expected to move toward a region of lower local velocities where its speed can balance the local velocity. Thus, it moves further away from the jet, toward the oxidizer side, in the upper direction.

In addition, the higher Z_{st} with ammonia addition, will also lead the flame to stabilize higher above the burner lip. Indeed, with ammonia addition, the flame will move toward a new stoichiometric contour $Z_{st,\,E>0} > Z_{st,\,E=0}$, located closer to the jet, in a higher-velocity region. It will thus need to move higher up along this line, in a lower-velocity region, allowing sufficient time for the diffusion of radicals and reactions to occur. Similar observations were done in the case of the fuel-side dilution of a methane jet with inert gas (CO_2, Ar, N_2) for which attached flame stabilization was observed closer to the jet centre and higher above the burner lip [24].

The present interpretation relies essentially on the aero-chemical couplings and their evolution with ammonia addition, which are expected to be dominant in the flame stabilization mechanism. This analysis should be however further developed, considering the evolution of thermo-diffusive properties of the gas in addition to their reactive properties. More specifically, the thermal and chemical interactions between the flame and burner and their evolution with ammonia addition should be considered.

The thermal interaction with the burner and their evolution with ammonia addition are thus further detailed in the next section 3.3. Chemical quenching to the burner lip, though not

investigated in the present study, might also contribute to some minor extent to the changes observed with ammonia addition. Indeed, the changes in the combustion chemistry induced by ammonia addition lead to a greater dependency in the presence of OH radicals relative to the larger dependency in H radicals in the methane flame [3,30]. This difference might trigger a different flame response in terms of chemical quenching to the burner lip. This effect is however expected to remain neglectable compared to the aero-chemical coupling or thermal interactions, particularly when considering that the mixtures investigated remains under $E = 0.3$ ($X_{NH3} = 0.52$), that the burner lip material employed is merely reactive (Al_2O_3) and the burner surface temperature is relatively low [28,31,32].

3.3. Effect of ammonia addition to heat transfer to the burner

It was observed that flame stabilization is particularly influenced by the modification in the aero-chemical coupling with ammonia addition. With the attached flame being in close contact with the burner, the thermal interactions of the flame with the burner should also be carefully investigated. More specifically, and as recalled in section 3.1, regime I can be subdivided into two considering the evolution of the temperature at the burner lip, T_{lip}, and the conductive heat flux in the burner lip from the surface, Φ, as shown in Fig. 9.

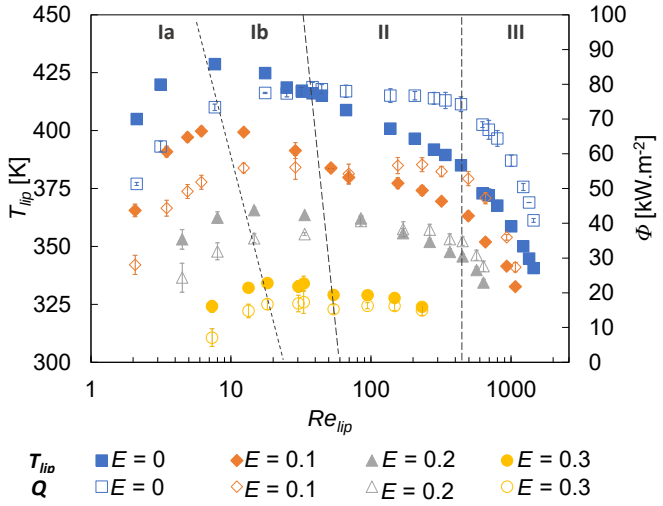

Figure. 9. T_{lip} and Q as a function of Re_{δ} for gradual ammonia addition.

A clear decrease of both T_{lip} and Φ is observed as ammonia is introduced whatever the jet velocity. However, the trends observed in the present work when increasing the jet velocity for the different E are similar to those observed in previous work on methane [28]. The large decrease of temperature observed at the burner lip can be explained by the decrease in the flame temperature with ammonia addition, as recalled in Table 1, and the increase in the flame-burner distance, d_a.

As a first approach, and to understand the relative importance of those parameters on the burner lip temperature variations, the variations with E of the adiabatic flame temperature, T_{ad}, obtained from 1D calculations [29], the maximum flame temperature, T_{max}, observed from experimental temperature mapping, and the burner lip temperature, T_{lip}, are introduced in Fig. 10. It can be seen that the adiabatic flame temperature variation, ΔT_{ad}, remains under 5 % in

the range $E = 0 – 0.3$. Similarly, the temperature mapping of the flame in the four different regimes (Ia, Ib, II, III) gives similar variation order (3 – 4 %). However, the variation of the maximum burner temperature, $\Delta T_{max,\,lip}$, is more than 20 % and the flame temperature variations alone seem insufficient to explain this drop.

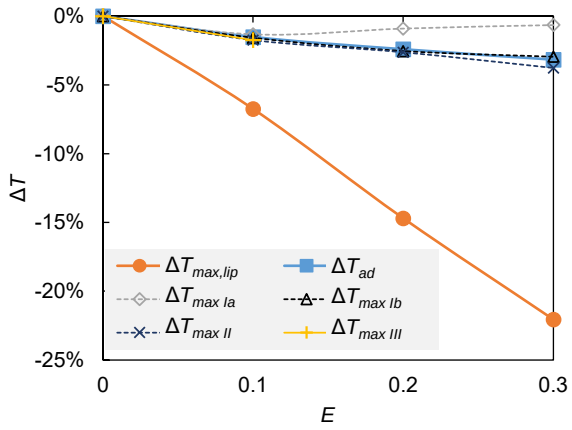

Figure 10. Flame and burner lip temperature variations with ammonia addition. Maximum flame temperatures from temperature mapping were taken at constant velocity in regimes Ia, Ib, II and III.

As observed in the previous section, the flame tip position varies with ammonia addition and the changes in the local aero-chemical coupling. This change in position is expected to affect the thermal interaction with the burner. The relationship between the burner lip temperature, T_{lip}, and the distance flame-burner, d_a, is introduced in Fig.11a for regime I and Fig.11b for regime II and III, for various E and U_J. It can be observed in Fig. 11a that in regime I, T_{lip} is well-correlated to d_a, with a temperature decreasing gradually as the flame gets more distant. In

regime II and III, as shown in Fig. 11b, the relationship is more complex. For each E, a large decrease of the temperature is observed as U_J is increased whereas d_a remains close to constant. This important decrease in temperature corresponds to the larger transfer by convection as jet velocity is increased. Nonetheless, for a constant U_J, a decreasing trend is observed with an increasing d_a, also corresponding to the increase E. Flame-burner distance plays thus an important role in those regimes too.

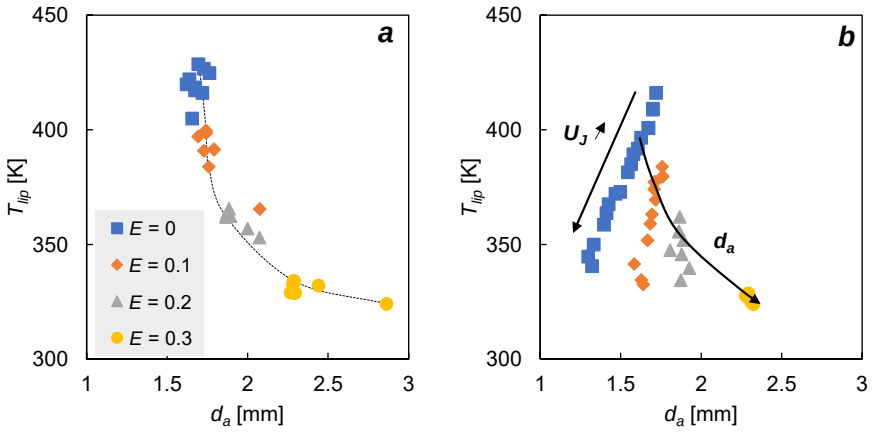

Figure 11. Burner lip temperature variations with the burner-flame distance for various E and U_J: (a) in regime I; (b) in regimes II and III.

The transition between regimes I and II, based on flame position, was observed for gradually larger MR_E as ammonia is introduced in Fig. 5. Similarly, the transition between Ia and Ib is observed for larger Re_{lip} when ammonia is introduced (from close to 10 for $E = 0$ to close to 20 for $E = 0.3$) as shown by the dashed lines in Fig. 9. The heat transfer is considered essentially

conductive in region I, so the larger Re_{lip} observed for the transition between Ia and Ib can be mostly attributed to the change in the flame position as explained in section 3.1.2. Indeed, the minimum d_a appears for gradually larger Re_{lip} within regime I as shown in Fig. 12. This minimum distance corresponding to larger transfer, explains the observation of the transition Ia to Ib for larger Re_{lip} as E is increased.

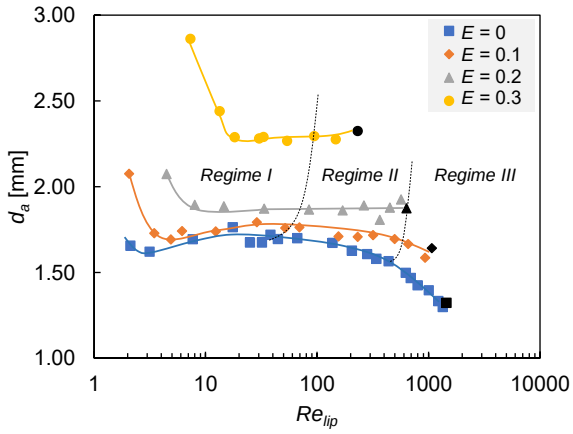

Figure 12. Flame-burner distance evolution along with the three aerodynamic regimes. The position just before liftoff is highlighted by black symbol.

3.4. Effect of ammonia on liftoff dynamics

After investigating the evolution of the stabilization dynamics of a methane attached flame with ammonia addition, we will now focus more specifically on the case of the liftoff, corresponding to the rupture of stabilization balance as described in the previous section 3.1 to 3.3. The extremum position, (R_E, H_E), and the position of the flame tip before liftoff, (R_{LO}, H_{LO}), are shown in the

normalized 1 x 1 domain above the burner lip in Fig. 13.

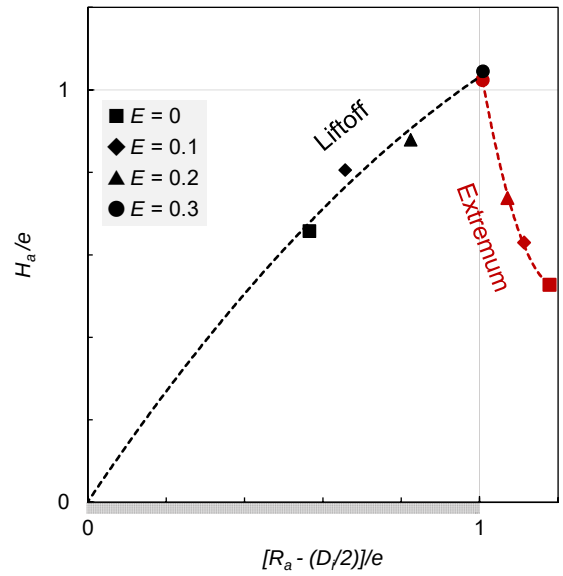

Figure 13. Evolution of the extremum position (red) and the position just before liftoff (black) for various E.

As developed in section 3.2, when ammonia is introduced in the mixture, the extremum position moves toward the jet, due to changes in the stoichiometric mixture fraction Z_{st}. For each E, when the jet velocity is increased from (R_E, H_E), the Z-contours are pushed toward the jet side where local velocities and strain rates are higher, up to local extinction and liftoff.

When E increases, this region becomes eventually more restricted, as observed from the convergence of the extremum position (R_E, H_E) and the position just before liftoff (R_{LO}, H_{LO}) in Fig. 13. The fact that the region becomes gradually more restricted and flame position constrained is also observable from the temperature gradients across the flame as represented in

Fig. 14. For $U_J = 2$ m·s^{-1}, in regime II, between the extremum position and the position just before liftoff, the introduction of ammonia leads to narrower temperature profiles, as observed from the shorter distance between the rises of the gradient close $r = 2$ mm and 8 mm. The maximum gradient on the air side remains similar order for all E but is gradually positioned closer to the burner lip, whereas it increases with E on the fuel jet side and is also positioned closer to the lip, the flame region getting narrower. The earlier liftoff can thus be associated with the lower flame burning velocity due to ammonia addition, restricting the stabilization region on the jet side, as well as the change in the local stabilization balance, particularly associated with the change in Z_{st}, which further restricts the domain on which flame can be stabilized on the oxidizer side.

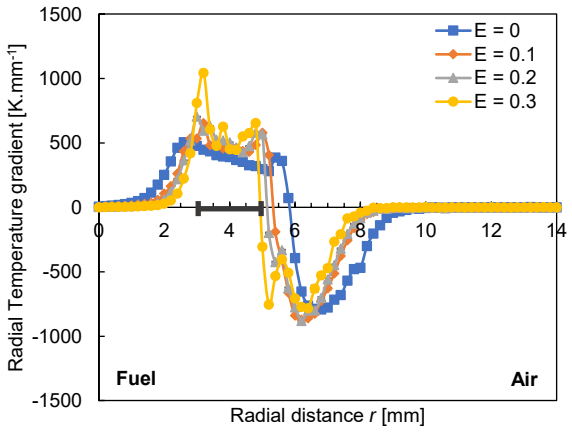

Figure 14. Radial temperature gradients across the flame at $z = 2$ mm, for various E in the regime II for $U_J = 2$ m·s^{-1}. The burner lip is denoted by a thick black line on the abscissa.

The extremum and liftoff line eventually reach each other close to $E = 0.3$, at the corner of the normalized 1 x 1 region, corresponding to a height close to the burner lip size (2 mm) and a radius corresponding to the outer edge of the burner lip. This mixing ratio particularly close to the blowoff limit observed on this burner ($E = 0.32$) [15]. When getting closer to this fuel mixing condition, if the jet velocity, U_J, is increased from the extremum position, the region in which flame can stabilize close to the burner is limited to a cornered point due to the higher velocities on the fuel side. The flame cannot stabilize anymore in the close-burner-region and it lifts from the burner. Besides, when the flame is in the extremum position, (R_E, H_E), the jet is laminar, and no air is yet dragged in the wake of the burner lip. The fuel-oxidizer mixing is thus expected to be particularly low in the shear layer above the burner lip. Those conditions will thus lead the flame to blowoff directly, as its base cannot stabilize, even at a higher position in the jet, with no region favorable in terms of both sufficiently low velocities and flammable mixtures.

4. Conclusions

The stabilization mechanisms of an ammonia/methane non-premixed jet flame were investigated experimentally in the present work using a local approach.

- When compared to the methane non-premixed jet flame, it could be observed that the flame position moves toward the jet and downstream as ammonia is added. This phenomenon can be understood as the effect of the increase in stoichiometric fraction, Z_{st}, leading the flame toward the fuel side, where mixing fraction is more favorable to its propagation; and the reduction of the mixture reactivity due to ammonia introduction, leading the flame to stabilizes further downstream where the local velocities are sufficiently low.
- The transition from regimes I to II was shown to be shifted to larger MR_E as ammonia is introduced into the mixture. This later transition could be associated with the higher fuel jet velocities that are necessary to drag sufficient air in the wake of the burner lip and cause a change in the position of the stoichiometric line Z_{st} up to the higher flame position. The momentum ratio MR, though representative of the overall dynamics at stake, cannot fully apprehend the local dynamics.
- The thermal interactions with the burner were shown to follow the same dynamics as defined in previous work [28], but the temperature at the burner decreased drastically as ammonia was introduced in the fuel jet, under the combined effect of flame temperature decrease and higher

attachment height. Moreover, similarly to the transitions between regimes I and II, the transitions between regimes Ia and Ib were observed for slightly larger local Reynolds numbers Re_{δ}. This could be associated with the evolution of the flame position with ammonia addition.

- Finally, it could be observed that as ammonia is introduced, the domain, in terms of attached flame position, on which the attached flame can stabilize get gradually reduced under the effects of the lower flame reactivity (and lower burning velocity) and the modification of the local stabilization dynamics evolution (particularly the position of the Z_{st} contours).

References

[1] J. Park, D.H. Lee, S.H. Yoon, T.M. Vu, J.H. Yun, S.I. Keel, Effects of Lewis number and preferential diffusion on flame characteristics in 80%H2/20%CO syngas counterflow diffusion flames diluted with He and Ar, Int. J. Hydrogen Energy. 34 (2009) 1578–1584.

[2] IEA, The Future of Hydrogen, Paris, 2019. https://www.iea.org/reports/the-future-of-hydrogen.

[3] H. Kobayashi, A. Hayakawa, K.D.K.A. Somarathne, E.C. Okafor, Science and technology of ammonia combustion, Proc. Combust. Inst. 37 (2019) 109–133.

[4] A. Valera-Medina, H. Xiao, M. Owen-Jones, W.I.F. David, P.J. Bowen, Ammonia for power, Prog. Energy Combust. Sci. 69 (2018) 63–102.

[5] G. Vezina, Y. Bicer, I. Dincer, C. Zamfirescu, F. Raso, Key Life Cycle Assessment Numbers for NH3, Green and Brown Energy, (2016). https://nh3fuelassociation.org/2016/08/24/key-life-cycle-assessment-numbers-for-nh3-green-and-brown-energy/ (accessed January 20, 2017).

[6] C. Mounaïm-rousselle, P. Brequigny, Ammonia as Fuel for Low-Carbon Spark-Ignition Engines of Tomorrow's Passenger Cars, Front. Mech. Eng. 6 (2020) 70.

[7] O. Kurata, N. Iki, T. Inoue, T. Matsunuma, T. Tsujimura, H. Furutani, M. Kawano, K. Arai, E.C. Okafor, A. Hayakawa, H. Kobayashi, Development of a wide range-operable, rich-lean

low-NOx combustor for NH3 fuel gas-turbine power generation, Proc. Combust. Inst. 37 (2019) 4587–4595.

[8] H. Lesmana, Z. Zhang, X. Li, M. Zhu, W. Xu, D. Zhang, NH3 as a transport fuel in internal combustion engines: A technical review, J. Energy Resour. Technol. Trans. ASME. 141 (2019) 1–12.

[9] E.C. Okafor, Y. Naito, S. Colson, A. Ichikawa, T. Kudo, A. Hayakawa, H. Kobayashi, Experimental and numerical study of the laminar burning velocity of CH4–NH3–air premixed flames, Combust. Flame. 187 (2018) 185–198.

[10] A. Ichikawa, Y. Naito, A. Hayakawa, T. Kudo, H. Kobayashi, Burning velocity and flame structure of CH 4 /NH 3 /air turbulent premixed flames at high pressure, Int. J. Hydrogen Energy. (2019) 1–9.

[11] X. Han, Z. Wang, M. Costa, Z. Sun, Y. He, K. Cen, Experimental and kinetic modeling study of laminar burning velocities of NH3/air, NH3/H2/air, NH3/CO/air and NH3/CH4/air premixed flames, Combust. Flame. 206 (2019) 214–226.

[12] S. Colson, Y. Hirano, A. Hayakawa, T. Kudo, H. Kobayashi, C. Galizzi, D. Escudié, Experimental and Numerical Study of NH3 /CH4 Counterflow Premixed and Non-premixed Flames for Various NH 3 Mixing Ratios, Combust. Sci. Technol. (2020), https://doi.org/10.1080/00102202.2020.1763326.

[13] A. Hayakawa, Y. Arakawa, R. Mimoto, K.D.K.A. Somarathne, T. Kudo, H. Kobayashi, Experimental investigation of stabilization and emission characteristics of ammonia/air premixed flames in a swirl combustor, Int. J. Hydrogen Energy. 42 (2017) 14010–14018.

[14] E. Rohde, K.R. Löblich, F. Fetting, The stabilization of turbulent ammonia-air flames on flameholders, Combust. Flame. 13 (1969) 327–329.

[15] S. Colson, M. Kuhni, C. Galizzi, D. Escudié, H. Kobayashi, Study of the Combined Effect of Ammonia Addition and Air Coflow Velocity on a Non-premixed Methane Jet Flame Stabilization, Combust. Sci. Technol. (2020), https://doi.org/10.1080/00102202.2020.1830276.

[16] K.M. Lyons, Toward an understanding of the stabilization mechanisms of lifted turbulent jet flames: Experiments, Prog. Energy Combust. Sci. 33 (2007) 211–231.

[17] C.J. Lawn, Lifted flames on fuel jets in co-flowing air, Prog. Energy Combust. Sci. 35 (2009) 1–30.

[18] F. Takahashi, W.J. Schmoll, Lifting criteria of jet diffusion flames, Symp. (Int.) Combust. 23 (1991) 677–683.

[19] F. Takahashi, M. Mizomoto, S. Ikai, N. Futaki, Lifting mechanism of free jet diffusion flames, Symp. (Int.) Combust. 20 (1985) 295–302.

[20] F. Takahashi, L.P. Goss, Near-field turbulent structures and the local extinction of jet

diffusion flames, Symp. (Int.) Combust. 24 (1992) 351–359.

[21] F. Takahashi, W.J. Schmoll, V.R. Katta, Attachment mechanisms of diffusion flames, Symp. (Int.) Combust. 27 (1998) 675–684.

[22] S. Lamige, J. Min, C. Galizzi, F. André, F. Baillot, D. Escudié, K.M. Lyons, On preheating and dilution effects in non-premixed jet flame stabilization, Combust. Flame. 160 (2013) 1102–1111.

[23] Y. Otakeyama, T. Yokomori, M. Mizomoto, Stability of CH4-N2/air jet diffusion flame for various burner rim thicknesses, Proc. Combust. Inst. 32 (2009) 1091–1097.

[24] M. Marin, F. Baillot, Experimental study of the lifting characteristics of the leading-edge of an attached non-premixed jet-flame: Air-side or fuel-side dilution, Combust. Flame. 171 (2016) 264–280.

[25] E.T. Child, K. Wohl, Spectrophotometric studies of laminar flames—I the decay of radical radiation, Symp. (Int.) Combust. 7 (1958) 215–220.

[26] D. Giassi, S. Cao, B.A. V. Bennett, D.P. Stocker, F. Takahashi, M.D. Smooke, M.B. Long, Analysis of CH* concentration and flame heat release rate in laminar coflow diffusion flames under microgravity and normal gravity, Combust. Flame. 167 (2016) 198–206.

[27] S. Lamige, Analysis of the influence of thermal boundary conditions on nonpremixed flame stabilization, Ph.D Thesis, INSA de Lyon, 2014 (in French). https://tel.archives-

ouvertes.fr/tel-01149918

[28] S. Lamige, K.M. Lyons, C. Galizzi, F. André, M. Kühni, D. Escudié, Burner lip temperature and stabilization of a non-premixed jet flame, Exp. Therm. Fluid Sci. 56 (2014) 45–52.

[29] Ansys CHEMKIN-PRO, Chemistry Simulation Software, 2021, https://www.ansys.com/products/fluids/ansys-chemkin-pro.

[30] S. Colson, A. Hayakawa, T. Kudo, H. Kobayashi, Extinction characteristics of ammonia/air counterflow premixed flames at various pressures, J. Therm. Sci. Technol. 11 (2016) JTST0048.

[31] S. Prakash, N.G. Glumac, N. Shankar, M.A. Shannon, OH concentration profiles over alumina, quartz, and platinum surfaces using laser-induced fluorescence spectroscopy in low-pressure hydrogen/oxygen flames, Combust. Sci. Technol. 177 (2005) 793–817.

[32] K.T. Kim, D.H. Lee, S. Kwon, Effects of thermal and chemical surface-flame interaction on flame quenching, Combust. Flame. 146 (2006) 19–28.

Acknowledgment

Funding:

A part of the work was carried out under the Collaborative Research Project of the Institute of Fluid Science, Tohoku University and in the framework of the Japan-France International Associated Laboratory (LIA) ELyT Global.

CRediT authorship contribution statement:

Sophie Colson:

Investigation, Formal analysis, Visualization, Writing – Original Draft

Manuel Kuhni:

Conceptualization, Methodology, Writing - Review & Editing, Funding acquisition

Akihiro Hayakawa:

Supervision, Writing - Review & Editing, Funding acquisition

Hideaki Kobayashi:

Supervision, Writing - Review & Editing, Funding acquisition

Cédric Galizzi:

Conceptualization, Methodology, Supervision, Writing - Review & Editing, Funding acquisition

Dany Escudié:

Conceptualization, Methodology, Supervision, Writing - Review & Editing, Funding acquisition